1 **Sialylation of Asparagine 612 inhibits Aconitase activity during mouse sperm capacitation;**

2 **A possible mechanism for the switch from oxidative phosphorylation to glycolysis.**

3 Ana Izabel Silva Balbin Villaverde[1], Rachel Ogle[1], Peter Lewis[2], Louise Hetherington[1], Vince

4 Carbone[3] Tony Velkov[4], Jacob Netherton[1], Mark A. Baker[1]

5 [1] Priority Research Centre in Reproductive Science, School of Environmental and Life Sciences,

6 University of Newcastle, Callaghan, NSW, Australia

7 [2] Centre for Chemical Biology and Clinical Pharmacology, Department of Biology, School of

8 Environmental & Life Sciences, The University of Newcastle, Callaghan

9 [3] AgResearch, Grasslands Research Centre, Tennent Drive, Private Bag 11008, Palmerston

10 North 4442, New Zealand.

11 [4] Faculty of Pharmacy and Pharmaceutical Sciences, Monash University, NSW, Australia

12

15

16 Correspondence: Mark A. Baker, Priority Research Centre in Reproductive Science, School of

17 Environmental and Life Sciences, University of Newcastle, Callaghan, NSW 2308, Australia.

18 Tel: +61 2 4921 6143: Fax: +61 2 4921 6308 E-mail: Mark.Baker@newcastle.edu.au

19

20

Abstract

22 After ejaculation, mammalian spermatozoa must undergo a process known as capacitation in order

23 to successfully fertilize the oocyte. Several post-translational modifications occur during

24 capacitation, including sialylation, which despite being limited to a few proteins, seems to be

25 essential for proper sperm-oocyte interaction. Regardless of its importance, to date, no single study

26 has ever identified nor quantified which glycoproteins bearing terminal sialic acid (Sia) are altered

27 during capacitation. Here we characterize sialylation during mouse sperm capacitation. Using

28 tandem mass spectrometry coupled with liquid chromatography (LC-MS/MS), we found 142 non-

29 reductant peptides, with 9 of them showing potential modifications on their sialylated

30 oligosaccharides during capacitation. As such, N-linked sialoglycopeptides from C4b-binding

31 protein, endothelial lipase (EL), serine proteases 39 and 52, testis-expressed protein 101 and

32 zonadhesin were reduced following capacitation. In contrast, mitochondrial aconitate hydratase

33 (aconitase; ACO2) was the only protein to show an increase in Sia content during capacitation.

34 Interestingly, while the loss of Sia within EL (N62) was accompanied by a reduction in its

35 phospholipase A_1 activity, the increase of sialylation in the ACO2 (N612) also resulted in a

36 decrease of the activity of this TCA cycle enzyme. The latter was confirmed by N612D

37 recombinant protein with both His and GFP tag, in which the N612D mutant had no activity

38 compared to WT when protein. Computer modelling show that N612 sits atop the catalytic site of

39 ACO2. The introduction of sialic acid causes a large confirmation change in the alpha helix,

40 essentially, distorting the active site, leading to complete loss of function. These findings suggest

41 that the switch from oxidative phosphorylation, over to glycolysis that occurs during capacitation

42 may come about through sialylation of ACO2.

51

Introduction

53   Sperm capacitation is a phenomenon first described by Chang, who demonstrated that freshly

54   ejaculated spermatozoa are unable to fertilize the oocyte immediately [1]. Rather, a period within

55   the female reproductive tract was required [1]. During this period, it is evident that spermatozoa

56   undergo a series of biochemical and metabolic changes to become fully capable of fertilizing the

57   egg [2-4]. From a metabolic perspective, Fraser and Lane first described the phenomenon of a

58   metabolic switch that occurs during capacitation [5]. In this context, freshly ejaculated

59   spermatozoa have high rates of oxygen consumption, however, during *in vitro* capacitation, mouse

60   spermatozoa decrease their reliance on oxidative phosphorylation and switch over to a glycolytic

61   pathway [5]. Using different metabolic substrates, this "switch" was shown to be necessary to

62   achieve fertilization [5]. In addition, the reliance on glycolysis explain why sperm-specific

63   glycolytic knockout mice, including GADPH [6], are infertile due to poor motility. From a

64   biochemical perspective, it is unknown how sperm make this switch. However, considering that

65   spermatozoa are transcriptionally and translationally silent, with the exception of mitochondrial

66   proteins [7], we reasoned that post-translational modifications of existing proteins would likely

67   play a role [8].

68   Whilst the role of phosphorylation in sperm capacitation is well studied [9-11], few studies have

69   looked at the specific role of protein glycosylation. The latter is characterized by the addition of

70   oligosaccharide side chains via a covalent linkage either at the asparagine (Asn) residue (N-linked)

71   or at the serine/threonine (Ser/Thr) residues (O-linked). There are a number of variations in terms

72   of glycan structures, which is translated in a wide range of biological functions [12, 13]. Notably,

73   terminal sugar sequences are among the features suggested as mediators of more specific roles

74   [12]. In this context, sialic acid (Sia), a monosaccharide with a nine-carbon backbone and

75   negatively charged, is considered an important terminal sugar.

76   The presence of Sia residues in glycoconjugates at the sperm surface seems to be vital for the

77   success of fertilization. Indeed, in both humans [14] and boars [15] with unexplained infertility or

78   subfertility, a decreased affinity for the lectin wheat germ agglutinin (WGA) has been reported,

79   suggesting either N-acetyl glucosamine and Sia residues are lacking within these cells.

80   Interestingly, surface Sia residues have also been shown to help sperm to survive and migrate

81   inside the female reproductive tract by reducing their phagocytosis and antigenicity [16-18] and

82   by helping them to penetrate the cervical mucus [19]. During sperm capacitation, it has been

83   suggested that Sia residues are shed from the surface of spermatozoa. In this context, studies using

84   lectin binding [20-23], surface charge determination [24, 25] radiolabeling of terminal sialyl

85   residues [26] and HPLC measurement following acid hydrolysis [27] have all indicated that

86   surface sialoglycoconjugates are probably lost or modified when spermatozoa are incubated under

87   capacitating conditions. One model that has been put forward is that the shedding of Sia residues

88   may be triggered by the release of neuraminidases present at the sperm surface [27]. If this is the

89   case, then the presence of oviduct fluid components [21] heparin [22] and/or albumin [28] in the

90   medium probably facilitate this release [27].

91   Despite the data that show changes in sperm sialylation content during capacitation, no single

92   publication has ever look at which proteins are sialylated in spermatozoa, yet alone quantified their

93   levels during capacitation. With this in mind, we used titanium dioxide (TiO$_2$) followed by peptide-

94   N-glycosidase F (PNGase F) cleavage to search for N-linked Sia-containing peptides and to

95   quantify them during *in vitro* capacitation of mouse sperm. In addition, we further studied both

96   mitochondrial aconitate hydratase (aconitase; ACO2) and endothelial lipase (EL) proteins to

97   demonstrate a biologically meaningful effect of the Sia residue during sperm capacitation.

98

Material and Methods

100   *Materials*

101   Chemicals were purchased from Sigma-Aldrich at highest research grade with the exception of the

102   following products. Chloroform was purchased from Fronine (Riverstone, NSW, Australia). The

103   2-D quant kit was from G.E. Healthcare (Castle Hill, NSW, Australia). BCA assay kit was from

104   Quantum Scientific (Pierce, Milton, QLD, Australia). HEPES was from Invitrogen Australia

105   (Melbourne, VIC, Australia). Sequencing grade trypsin was supplied by Promega (Alexandria,

106   NSW, Australia). Antarctic phosphatase and PNGase F were purchased from New England

107   Biolabs (Arundel, QLD, Australia). Phospholipase A$_1$ selective substrate (PED-A$_1$) (N-((6-(2,4-

108   DNP)Amino)Hexanoyl)-1-(BODIPY® FL C5)-2-Hexyl-Sn-Glycero-3-Phosphoethanolamine)

109   was purchased from Molecular Probes (Melbourne, VIC, Australia). The TiO$_2$ was collected from

110   a disassembled column. Ionophore A23187 was purchased from Calbiochem (EMD Biosciences,

111   La Jolla, USA).

112

113   *Sperm collection and in vitro capacitation*

114   Animal use was approved by institutional and New South Wales State Government ethics

115   committees. Adult Swiss mice (~8-10 weeks) were euthanized and the epididymides were

116   removed. Sperm cells were recovered from the cauda of the epididymides using retrograde

117   flushing [29, 30] and then incubated for 10 min at 37°C in 0.3% BSA BWW media to allow cell

118   dispersion [31]. For the non-capacitated group, sodium bicarbonate was replaced by sodium

119   chloride in the BWW media. Pentoxifylline and dibutyryl-cAMP (dbcAMP) were added only in

120   the capacitated group at a final concentration of 1mM each. All samples were incubated for 60 min

121   at 37°C and then sperm cells were washed three times (300 x g, 3 min) using BWW media without

122   BSA.

123

124   *Protein extraction and sialoglycopeptide enrichment*

125   Sperm pellets were resuspended in a lysis buffer consisting of 1% (w/v) C7BzO [3-(4-Heptyl)

126   phenyl-3-hydroxypropyl) dimethylammoniopropanesulfonate], 7 M urea, 2 M thiourea, and 40

127   mM Tris (pH 10.4) at a final concentration of ~2.5 x 10^6/ 100 µL and incubated for 1 h (4°C) with

128   constant rotation. Supernatant (18,000 x g, 15 min, 4°C) was recovered and total protein was

129   quantified using a 2-D quant kit following manufacture's protocol. Proteins were reduced (10 mM

130   DTT, 30 min, 30°C), alkylated (45 mM iodoacetamide, 30 min, 30°C) and 250 µg of protein was

131   precipitated using methanol and chloroform [32]. Samples were incubated overnight (37°C) with

132   trypsin at a 1:50 (trypsin/protein) ratio. Proteases were inactivated (bath sonication, 15 minutes)

133   and peptides were treated with alkaline phosphatase (20 U, 2 hours, 30°C).

134   Enrichment of glycopeptides containing terminal Sia was performed as previously described [33].

135   In brief, peptide samples were diluted in loading buffer [1 M glycolic acid, 80% (v/v) ACN, 5%

136   (v/v) TFA] and then applied to TiO_2 beads (2 mg). After incubation for 1 h, TiO_2 beads were

137   washed [washing buffer 1; 80% (v/v) ACN, 1% (v/v) TFA, and washing buffer 2; 20% (v/v) ACN,

138   0.1% (v/v) TFA] and dried in a vacuum concentrator. Enzymatic deglycosylation of N-linked

139   sialoglycopeptides was performed with 1 µL of PNGase F for 3h at 37°C. Released peptides were

140   recovered, dried, resuspended in 0.1% (v/v) TFA and then loaded on a LC-MS (AmaZon ETD Ion

141   Trap; Bruker Daltonik, Bremen, Germany) with an online-nanosprayer, and run as previously

142   described [34].

143

144   *Bioinformatics*

145   Acquired CID spectra were processed in DataAnalysis 4.0; deconvoluted spectra were further

146   analyzed with BioTools 3.2 software and submitted to Mascot database search (Mascot 2.2.04,

147   Swissprot database (546439 sequences; 194445396 residues, release date 19/20/14)). The

148   following variable modifications have been used: phosphorylation (STY), carbamidomethylation

149   (C), deamidation (NQ) and oxidation (M). To identify N-linked glycosylation sites, a deamidated

150   Asn residue had to be flanked by the glycosylation consensus motif (NXS/T, where X is any amino

151   acid besides proline) which was manually validated. Peptides that were assigned a deamidation

152   event based solely on the MS data (i.e., no *y-* or *b-* fragment ion for a particular deamidated Asn

153   residue could be detected) were presumed to be glycosylated only if a canonical N-glycan motif

154   was present.

155   The derived mass spectrometry datasets on the 3D-trap system were combined into protein

156   compilations using the ProteinExtractor functionality of Proteinscape 2.1.0 573 (Bruker Daltonics,

157   Bremen, Germany). In order to exclude false positive identifications, peptides with Mascot scores

158   below 40 were rejected. Peptides with a mascot score above 40 were manually validated in

159   BioTools (Bruker Daltonics, Bremen, Germany) on a residue-by residue basis using the raw data

160   to ensure accuracy as previously described [33]

161

162   *Peptide label-free quantification*

163   MS-based label-free quantification of the N-glycopeptides identified was performed using the

164   software Data Analysis 4.1 (Bruker Daltonik GmbH, Bremen, Germany). Peptides were matched

165   based on charge state, m/z value and elution time. The match was confirmed by visual inspection

166   of the peptide on the survey view and by manual comparison of the MS/MS spectra if available.

167   Relative peptide quantification was carried out by integrating the area of the extracted ion

168   chromatograms (XIC) of the monoisotopic peak from MS spectra (Fig. 1) [33]. For peptide

169   quantification, four biological replicates, each consisting of pooled samples from 3-4 mice, were

170   run.

171

172

173

174 *PLA1 activity assay*

175 The phospholipase A_1 (PLA_1) activity of EL in intact mouse spermatozoa was analyzed using a

176 dye labeled-PLA_1 specific substrate [35]. Sperm samples were divided into six groups; non-

177 capacitated with or without H89 or A23187 and capacitated with or without H89 or A23187. The

178 compound H89 was supplemented 10 min prior to the addition of pentoxifylline and dbcAMP.

179 After capacitation for 1h, ionophore A23187 was added to cells (20 µM final concentration) after

180 30 min of incubation and then samples were allowed to incubate for another 30 min. Spermatozoa

181 were washed (300 x g, 3 min) twice using BWW media with BSA and then once with BWW media

182 without BSA. Sperm pellets were then resuspended in BWW media without BSA to a final

183 concentration of 20 x 10^6 sperm/ mL.

184 A stock solution of PED-A_1 substrate (5 mM in DMSO) was diluted (1:625) with BWW medium

185 without BSA yielding a final concentration of 8 µM. Aliquots of 25 µL of the PED-A_1 working

186 solution were placed in a v-bottom 96-well plate and then 25 µL of the sperm samples was added.

187 Controls included wells containing only PED-A_1 solution or sperm cells. The plate was incubated

188 at 37°C and fluorescence measurements were taken every 30 sec during a 1h-period using the

189 microplate reader FLUOstar OPTIMA (BMG Labtech, Mornington, VIC, Australia) with

190 excitation and emission wavelengths of 485 and 510 nm, respectively. Linear regression was

191 calculated using the average results for the first 10 min of reading and reaction rates (slope) were

192 calculated for each sample. PLA_1 activity was assessed in five independent experiments.

193

194

195

196   Aconitase Vectors

197   ACO2 cDNA was ligated into the pcDNA3-EGFP plasmid. Primers were designed to have HindIII

198   (forward) and NotI (reverse) restriction sites as well as 8 extra base pairs on the ends to allow

199   enzyme cleavage. Two different reverse primers were used to create two different plasmids, the

200   first containing a linker sequence to create an ACO2-EGFP fusion, and the second containing a

201   linker sequence followed by a (HIS)$_6$-tag and stop codon to create his-tagged ACO2. This was

202   achieved using mouse cDNA and the following overhanging primers:

203   Forward: ACGAATTC–AAGCTT–ATGGCGCCTTACAGCCTCCTGGT

204   Reverse 1: GGTGCTTA–GCGGCCGC–GAGCTTCCACCACCTCC–

205   CTGCTGCAGCTCCTTCATCCTGTTG

206   Reverse 2: GGTGCTTA–GCGGCCGC–TCA–

207   ATGGTGGTGGTGATGATGGCTTCCACCACCTCC–

208   CTGCTGCAGCTCCTTCATCCTGTTG

209   For PCR, Thermo Scientific Phusion High-Fidelity DNA Polymerase was used and their

210   instructions followed. Each 20 µl PCR was made up with the following concentrations: 1 x HF

211   buffer, 200 µm dNTPs, 0.5 µM each of forward and reverse primer, ~100 ng DNA, 3% DMSO

212   and 1 unit Phusion polymerase. PCR conditions were: 98°C for 30 sec, [98°C for 10 sec, 65°C for

213   30 sec, 72°C for 2 min] x 35 cycles, 72°C for 10 min. Annealing temperature was optimized at

214   65°C for both sets of primers.

215   PCR inserts and pcDNA3-EGFP vector were digested with Promega enzymes; NotI and HindIII

216   after Wizard mini-prep kit clean-up. Insert and vector were ligated at a 3:1 ratio using Promega T4

217   DNA ligase and then transformed into E. coli cells on ampicillin agar plates. Singles colonies were

218   cultured the following day and then plasmids extracted. Plasmids were again digested with HindIII

219   and NotI to check for insertions and the ones containing inserts were sent away for Sanger

220   sequencing using four sequencing primers to cover entire insert and check for mutations:

221   GGACTTTCCAAAATGTCG, AGGCCGAACAGACATTGC, AGATGCAGACGAGCTTCC,

222   TTCATCCAGTGGACAAGC.

223

224   *Site directed mutagenesis*

225   To mimic the negative charge of the Sia modification on ACO2, we changed the amino acid 612

226   (Asn or N) to aspartic acid (D) using site directed mutagenesis. A single base pair change on

227   chr15:81913178 to change the codon from AAC to GAC was achieved using the following

228   primers:

229   Forward: TGCTCATCGGTGCCATCAACATC

230   Reverse: GGTTGTTAGAGATGTCATCCAGATGCCCAC

231   Phusion DNA Polymerase PCR was done using the same reaction as written in the above methods

232   and the PCR conditions as follows: 98°C for 3 min, [98°C for 10 sec, 64 °C for 30 sec, 72°C for 6

233   min] x 35 cycles, 72°C for 10 min. Following PCR, the plasmid bands were cut out of an agarose

234   gel, purified and digested with DpnI from NEB. Following another clean-up step, the plasmids

235   were transformed into E. coli and grown on agar plates overnight. Single colonies were selected

236   the following day and cultures grown overnight. Plasmids were extracted from these colonies and

237   sent   away   for   sequencing   to   check   for   mutation   using   sequencing   primer

238   AGATGCAGACGAGCTTCC.

239 *Transfection*

240 HEK293T cells were used for transfection with ACO2-EGFP plasmid and ACO2-(HIS)$_6$ plasmid

241 including the WT and N612D versions of these plasmids. We confirmed that human cells would

242 be suitable for transfection with the mouse ACO2 gene due to almost identical sequences. Cells

243 were split into 6-well plates to attain ~50% confluence the following day. Transfection was done

244 with 5 μg plasmid DNA and 10 μg PEI in 3 mL media. Firstly, 5 μg of plasmid and 10 μg PEI

245 were put into separate tubes and 150 μL DMEM (no FBS) added to each one. These were then

246 mixed together and incubated for 30 min. Next, media in the 6-well plates was replaced with 2.7

247 mL of fresh DMEM and the 300 μL DNA:PEI mix added. Cells were left to transfect for the times

248 indicated and then harvested. ACO2-GFP cells were fixed using 4% paraformaldehyde for

249 microscopy and FACS analysis or frozen at -80°C for immunoblotting. ACO2-(HIS)$_6$ cells were

250 frozen at -80°C for immunoblotting or Aconitase assay.

251

252 *Aconitase Assay*

253 Aconitase assay from BioVision was used with adjusted methods.

254 Day 1: Frozen transfected HEK293T cells consisting of (HIS)$_6$-wild-type ACO2 transfected (WT)

255 and N612D mutant and control non-transfected cells were thawed on ice. Cells were resuspended

256 in 400 mL lysis buffer (PBS pH 8, 10 mM imidazole, 0.5% tween) and then sonicated and

257 centrifuged (16,000 g, 4°C) for 15 min. A 200 μL aliquot of N612D and control samples were

258 placed in fresh tubes and the rest discarded. The WT samples were split into 3 tubes: 200 μL, 100

259 μL and 50 μL. A 200 μL of lysis buffer and then 50 μL Ni-NTA agarose beads were added and

260 samples rolled for 1 h at 4°C. Beads were washed thrice in wash buffer (PBS pH 8, 20 mM

261 imidazole, 0.5% tween) and once in kit assay buffer. Afterwards, beads were resuspended in 100

262 µL kit assay buffer, 10 µL activation solution was added, and samples were rolled for 1 h at 4°C.

263 One hundred µL of reaction mix was added to each tube and samples rolled at room temperature

264 overnight.

265 Day 2: Frozen non- and capacitated sperm cells were thawed on ice. Cells were resuspended in

266 100 µL kit assay buffer, sonicated and centrifuged (16,000 g; 4°C) for 15 min. Ten µL of activation

267 solution was added and samples incubated for 1 h on ice. Afterwards, 100 µL reaction mix was

268 added to each tube and samples incubated at room temperature for 2.5 h. Standards were made

269 according to instructions and allowed to incubate for 30 min. The beads from day-1 preparation

270 were centrifuged and, together with the non- and capacitated sperm prepared on day 2, were loaded

271 in a 96-well plate in 100 µL duplicates. Ten µL of developer was added, samples incubated at

272 room temperature 25°C and read at 450 nm.

273 Following kit, nickel bead enrichment, $(HIS)_6$-recombinant protein were eluted with 250 mM

274 imidazole and then frozen along with non- and capacitated samples. For immunoblotting, samples

275 were methanol/chloroform precipitated and lysed in SDS-PAGE buffer.

276

277 *SDS-PAGE and immunoblotting*

278 Non-capacitated and capacitated mouse spermatozoa (with and without H89) were prepared as

279 described above and then diluted in SDS-PAGE buffer. Protein (10 µg) was separated by SDS-

280 PAGE using 4-20% precast polyacrylamide gels (NuSep Ltd, Lane Cove, NSW, Australia) and

281 then transferred onto nitrocellulose membrane Watman® Optitran® BA-S 85 (GE Healthcare,

282 Castle Hill, NSW, Australia). The membrane was blocked (1 h at room temperature) and incubated

283   overnight at 4°C with rabbit polyclonal antibody raised against EL (orb100394, LIPG; Biorbyt) at

284   a dilution of 1:500 in 5% (w/v) skim milk TBS-T (0.02 M Tris, 0.15 M NaCl, 0.1% (v/v) Tween-

285   20; pH 7.6).

286   After three washes, membrane was incubated for 1 h at room temperature with anti-rabbit IgG

287   horseradish peroxidase (HRP) conjugate (Sigma-Aldrich) at a concentration of 1:1000 in 5% (w/v)

288   skim milk TBS-T. The membrane was washed thrice, and immuno-reacted proteins were detected

289   using an enhanced chemiluminescence (ECL) kit (Amersham International) according to the

290   manufacturer's instructions. Equal loading was confirmed by stripping the membrane and then re-

291   probing it with a mouse monoclonal anti-α-tubulin antibody.

292   To confirm the capacitation of sperm cells and the efficiency of H89 at inhibiting tyrosine

293   phosphorylation via PKA, samples were probed with the mouse monoclonal anti-

294   phosphotyrosine–peroxidase antibody PT66 (A5964; Sigma-Aldrich). Loading control was

295   performed using mouse monoclonal anti-α-tubulin antibody.

296   Immunoblots of WT and mutant ACO2 were essentially performed as previously described [34].

297   The following antibody dilutions were used: rabbit polyclonal anti-Aconitase 2 antibody at 1:1000

298   (ab83528; Abcam), rabbit polyclonal anti-6X His tag antibody at 1:1000 (ab1187; Abcam). All

299   secondary antibodies were used at a 1:1000 dilution. Anti-GFP was a kind gift from Peter Lewis

300   and used at 1:1000.

301

302   *Immunocytochemistry*

303   Capacitated and non-capacitated intact mouse spermatozoa were fixed in 4% (w/v) formaldehyde

304   for 10 min at room temperature. Cells were washed three times in PBS containing 0.5 M glycine,

305   immobilized on poly-L-lysine coverslips and permeabilized with ice cold methanol for 10 min.

306   Coverslips were washed, blocked for 1 h with 3% (w/v) BSA in PBS and incubated overnight with

307   anti-EL antibody in a 1:50 dilution with PBS containing 1% (w/v) BSA. Following three washes

308   with PBS, cells were incubated with Alexa Fluor® 488 goat anti-rabbit IgG (Life technologies) in

309   a 1:100 dilution with PBS containing 1% (w/v) BSA. Coverslips were washed as described above

310   and then mounted with Mowiol antifade medium. Cells were evaluated using phase contrast and

311   epifluorescence microscopy.

312

313   *Acrosomal status*

314   The acrosomal status of mouse spermatozoa was assessed either at time 0 (non-capacitated) or

315   following 30 min of capacitation (37°C; 5% CO_2). After 30 min of incubation, the ionophore

316   A23187 (10 µM final concentration in DMSO) or DMSO vehicle only were added and then cells

317   were incubated for 30 min. Samples were washed twice using PBS and 10 µl of sperm suspension

318   was spotted onto superfrost slides, spread with a glass pipette and air-dried. Slides were immersed

319   in absolute methanol for 15 min, rinsed with PBS and then incubated for 30 min with fluorescein

320   isothiocyanate-conjugated *Arachis hypogaea* peanut agglutinin (FITC-PNA) (15 µg/mL final

321   concentration). The slides were rinsed in PBS and mounted with antifade media. For each slide,

322   images of adjacent fields were recorded under a x40 magnification to achieve a sperm count of at

323   least 100 spermatozoa. Spermatozoa were classified into one of the three categories of FITC-PNA

324   labelling: I = intact acrosome; II = partial acrosome reaction; and III = complete acrosome reaction.

325   For each experimental condition, a minimum of 3 slides were examined and quantified.

326

327 *Statistical analysis*

328 The data obtained by MS-based label-free quantification were normalized among runs using the

329 average area of five different glycopeptides visually selected based on their quality and constant

330 intensity. The normalized area of each glycopeptide was then compared between non-capacitated

331 and capacitated sperm samples using student's *t*-test. Relative immunoreactivity for EL and α-

332 tubulin and sperm PLA_1 activity were compared among groups using paired *t*-test. P-values < 0.01

333 were considered as significant. Standard errors are shown in the graphs. The data for acrosome

334 reaction from 5 biological replicates were subjected to analysis of variance (two-way ANOVA)

335 followed by paired *t*-test. Data are shown as mean ± S.D. when not specified otherwise.

336

337 *Molecular modelling; Covalent docking model of Sialic acid binding of Asn612 to aconitate*

338 *hydratase*

339 Molecular docking experiments were carried out using the program GOLD (Genetic Optimization

340 for Ligand Docking) version 5.2 and favouring the CHEMPLP Scoring system (Verdonk 2003).

341 The three-dimensional iteration of Sialic acid (MolPort-008-267-866) was used for covalent

342 docking onto the identified target residue of Asn612 on a model of Aconitate hydratase,

343 mitochondrial precursor from *Mus musculus* (EC: 4.2.1.3) generated by the PHYRE2 protein

344 recognition server Kelley (2015). The proposed reaction mechanism and subsequent product is

345 depicted in Scheme 1. The size of the search domain was set to 10 Å and the covalent docking

346 function within GOLD was employed. Docking was executed using a 100% search efficiency,

347 generating ten Genetic Algorithm (GA) runs, while the rotameric states of several sidechains

348 including Gln563, Lys605 and Arg648 were set to library rotamer orientations and the remainder

349   of the site remained rigid. The generated binding poses were then inspected, and conformations

350   were chosen for further analysis taking into account their ranking and interactions with the probed

351   residues. Molecular visualizations were performed using the software package PYMOL

352   (Schrödinger, NY, USA).

353

354   **Results**

355   In order to determine the efficiency of the protocol used here to induce sperm capacitation, tyrosine

356   phosphorylation was measured (Fig. 1). As shown, tyrosine phosphorylation increased during

357   capacitation, which could be abrogate with the PKA inhibitor H89, suggesting that the sperm cells

358   used in this study were capacitating. The experimental paradigm used in this study was to compare

359   the changes associated with the capacitation process itself (Cap *vs* Cap-H, Fig. 2) as opposed to

360   changes over time (N-Cap *vs* Cap, Fig. 2).

361

362   *Sialylated glycoproteins identified in mouse sperm*

363   The protocol to enrich for sialylated N-linked glycopeptides is shown in Figure 2. Herein,

364   spermatozoa were obtained from the mouse epididymides, combined, and then separated into two

365   separate tubes. Whilst one tube had capacitating media, the other lacked sodium bicarbonate which

366   is essential for this process. The samples were washed, lysed and digested. Sialylated-glycoprotein

367   enrichment was performed using TiO_2 beads. Although this is not specific for glycopeptides, but

368   rather for negatively charged molecules, the elution through PNGase F treatment of the beads

369   allows the selection of N-linked glycopeptides generally or sialylated glycopeptides specifically.

370 Enrichment of sialylated N-linked glycopeptides using TiO_2 allowed the identification of 142

371 unique peptides, which were from 90 different glycoproteins (Table 1), demonstrating that some

372 proteins possessed N-linked glycopeptides with terminal Sia in more than one position. Of

373 particular interest, the characterization of the glycopeptides containing Sia residues represented

374 36.7% of the total non-reductant peptides identified by MS/MS. This is in perfect agreement with

375 our previous paper with rat sperm, in which around 34% of the peptides identified were classified

376 as glycopeptides after enrichment using TiO_2 [33].

377 Due to ion fragmentation patterns (i.e., no visualization of the *y-* or *b-* fragment ion for the

378 deamidated Asn), a precise identification of the residue containing the deamidation was not

379 possible in all cases. Hence, the peptides exhibiting ambiguous annotation of the deamidated

380 residue are indicated in Table 1 with an asterisk. Supplementary I contains MS/MS spectrum from

381 all peptides present in Table 1 whereas Supplementary II presents data such as measured m/z

382 values, peptide charge and retention times.

383

384 *Changes in sialylated N-linked glycopeptides during capacitation*

385 The data for label-free quantification of the N-linked glycopeptides in non-capacitated versus

386 capacitated sperm are shown in Table 1. Some glycopeptides were presented at very low amount,

387 impairing their quantification in some biological replicates. These cases are indicated in Table 1

388 as not determined (ND) since we were not confident to report these further. Of interest, nine (6.3%)

389 of the glycopeptides identified here underwent significant changes during sperm capacitation.

390 These glycopeptides belong to the proteins: ACO2, C4b-binding protein (C4BP), EL, inactive

391 serine protease 39 (PRSS39, also known as testicular-specific serine protease 1; TESP1), serine

392   protease 52 (PRSS52, also known as testicular-specific serine protease 3; TESP3), testis-expressed

393   protein 101 (TEX101) and zonadhesin (Table 1). Interesting, these glycopeptides were shown to

394   be reduced during capacitation except for the peptide from ACO2, a protein involved in the

395   tricarboxylic acid (TCA) cycle (Table 1).

396

397   *Determination of EL amount and sub-cellular localization*

398   In order to determine the consequences of sialylation changes during capacitation, we choose two

399   proteins for further study: the EL and ACO2. The EL has been reported as primarily having PLA_1

400   activity [36]. This was of particular interest, since changes in the composition of lipids from cell

401   membranes, such as the formation of lysophospholipids by phospholipids hydrolysis, are known

402   to modify membrane fluidity [37, 38] and function through the modulation of receptors [39],

403   channels [40, 41] and enzyme activity [42] within its structure. Considering that morphological

404   and functional changes in sperm membranes, including alteration in membrane fluidity, are

405   essential for capacitation [43] and that lysophospholipids may be involved in the modulation of

406   the acrosome reaction [44], we further investigated the behavior of EL during this process.

407   Immunoblotting for EL was performed, aiming to determine what happens to the entire protein

408   during capacitation. As shown in Figure 3, the total amount and the molecular weight of EL did

409   not change after capacitation (Fig. 3A, lanes 1 and 2). In addition, the use of the PKA inhibitor

410   H89 during capacitation also did not affect the amount of EL (Fig. 3A, lanes 2 and 3). To

411   demonstrate equal loading, we re-probed the sample with anti-α tubulin antibody (Fig. 3B). Using

412   the software Image J, the quantitative values of each band were plotted to confirm that no

413   significant change occur in EL expression after capacitation (Fig. 3C).

414   To verify whether the protein EL is redistributed in spermatozoa during capacitation, we

415   performed immunostaining using anti-EL antibody. Immunostaining for EL was observed in both

416   head and tail regions of non-capacitated (Fig. 4a,c) and capacitated (Fig. 4b,d) mouse sperm. For

417   both groups, the anterior acrosome region stained for EL whereas the equatorial region showed no

418   staining. In addition, the staining intensity of the postacrosomal sheath showed high variation

419   among cells; being absent in some cases (Fig. 4b, white arrow exemplifies this variation). In the

420   tail region, although the midpiece and the cytoplasmic droplet showed high staining for EL, we

421   noted that some cells exhibited weaker labeling of the midpiece (Fig. 4c,d). Of interest, the

422   percentage of these cells, with reduced immunoreactivity for EL at the midpiece, increased when

423   sperm was incubated in capacitating conditions (from around 7% to 68%). The same was observed

424   in samples capacitated with the PKA inhibitor H89, suggesting that the diminish in EL

425   immunofluorescence within the midpiece is independent of PKA (data not shown). Secondary only

426   controls showed no fluorescence (Fig. 4e,f).

427

428   *Loss in EL activity occurs during capacitation, independent of H89 and the acrosome reactions*

429   In order to determine if the loss of Sia residue on EL affected enzyme activity, we specifically

430   measured PLA_1 activity on both non- and capacitated spermatozoa. Furthermore, as the

431   immunofluorescence showed quite a varied pattern of EL expression, including acrosome location,

432   we wanted to see if the loss of the acrosome had any effect of the overall EL activity. Therefore,

433   we incubated sperm under non- or capacitating condition, with and without H89. Secondly, both

434   non- and capacitated spermatozoa were induced to undergo the acrosome reaction. These sperm

435   cells were subsequently washed, then the level of intact, partial or complete acrosome loss were

436 measured using FITC-PNA staining. As shown in Figure 5, capacitated sperm plus ionophore

437 A23187 had the highest level of complete acrosomal loss as expected.

438 To determine whether a change in EL activity occurred during capacitation, we measured PLA_1

439 activity before and after capacitation, together with the inhibitor H89 or the acrosomal-inducer,

440 ionophore A23187. We observed a significant loss in the PLA_1 activity of EL during capacitation

441 (Fig. 6A, bars N-cap *vs* Cap). An example of the loss in PLA_1 activity is demonstrated in Figure

442 6B. Here, two of the five biological replicates are shown over time from either non-capacitated

443 (solid line) or capacitated (dotted line) sperm populations. Addition of the PKA inhibitor H89,

444 which is commonly used to prevent capacitation, failed to abrogate the loss of PLA_1 activity (Fig.

445 6A, N-cap + H89 *vs* Cap + H89). Furthermore, the loss of the acrosome had no further bearing on

446 the reduction of the PLA_1 activity in EL, with acrosome-reacted capacitated spermatozoa (Fig. 6A,

447 bar Cap + A23187) having a similar activity to the capacitated (Fig. 6A, bar Cap) and the H89

448 "capacitated" (Fig. 6A, Cap + H89) cells. In all cases, the amount of activity was normalized to

449 the amount of endothelial lipase present with an immunblot.

450

451 *Sialylation of N612 inhibits ACO2 activity*

452 Spermatozoa are catabolic in nature and, as such, it is not a surprise that the majority of Sia residues

453 are lost during capacitation. However, in this study, we observed one enzyme that had an increase

454 in sialylation, namely ACO2. To further understand this finding, we measured total Aconitase

455 activity before and following mouse capacitation. As shown, during capacitation a statistically

456 significant decrease in the level of Aconitase activity was observed (Fig. 7). Although this

457 measurement would include both cytoplasmic and mitochondrial Aconitase activity, we reasoned

458   that sperm have very little cytoplasm, therefore, the bulk of Aconitase activity should be from the

459   mitochondrial form.

460   To confirm that a decrease in ACO2 activity occurs specifically through sialylation at N612, we

461   made both WT and Sia mimic, whereby the N612 was replaced by the negatively charged Aspartic

462   acid (N612D). In both cases (WT and mimic), we made a GFP- and a HIS-tagged separate proteins.

463   Expression of the GFP-tagged proteins showed both WT and mutant were expressed in the

464   mitochondria as expected (Fig. 8A-D). Of interest, under fluorescence microscopy, we also noted

465   a decrease in the level of GFP-tagged mutant, yet the number of cells transfected was equal

466   (compare Fig. 8A and 8B). To support this, we ran the cells through flow-cytometry. Analysis

467   demonstrated that, in every replicate, the same number of cells were transfected (on average 35%),

468   however, the mean level of GFP-fluorescence was significantly lower in the N612E-Aconitase

469   expressing cells. For example, the histogram on Figures 8C and 8D demonstrates that the peak

470   height for GFP fluorescence in WT is slightly higher (Fig. 8E, black downward arrow) than in the

471   N612E mutant (Fig. 8F, black downward arrow). This suggests that cells are less favorable to the

472   expression of the N612E mutant over the WT. To confirm this hypothesis, we ran a SDS gel,

473   transferred and probed it with antibodies against GFP- (not shown) or $(His)_6$-tagged proteins (Fig.

474   9A,B). As shown, WT ACO2 is more abundant than the mutant form (Fig. 9A,B; compare lanes 1

475   to 4). From our estimation, the N612E expression is between 25-50% of that of WT (see lanes 3

476   and 4 *vs* 5).

477   We next measured the ACO2 activity of the WT and N612E mutant (Fig. 10). The use of equal

478   amounts of recombinant protein was confirmed by immunoblotting. Remarkably, even when left

479   overnight, we were unsuccessful in obtaining any ACO2 activity from the N612E mutant. In

480   contrast, we could easily detect WT ACO2 activity. When put together, these datasets suggest that

481   a switch in the ACO2 activity occurs during capacitation. This change in activity pattern is likely

482   related to the modifications in the metabolic pathways described during the capacitation of mouse

483   spermatozoa (i.e., from the oxidative phosphorylation pathway to the glycolytic pathway).

484   *Modelling the bound sialoglycoprotein to Aconitate hydratase*

485   To understand the impact sialation would have on N612, we modelled the effect. Published crystal

486   structures of Aconitate hydratase [45-48] and our highly homologous model, describes a large

487   macromolecular structure comprising of four distinct domains employing a [4Fe-4S] cluster to

488   catalyse the stereospecific dehydration of citrate to isocitrate [49]. Within the enzyme itself, sits

489   several highly conserved amino acids, such as Asp192, His194 and Arg607 that are crucial for

490   ACO2 activity (shown in Fig. 11). N612 resides on a short α-helical element immediately atop the

491   active site, in an area often denoted as domain 4 [50]. In order to fit a sialic acid residue with N612,

492   multiple changes in rotamers of sidechains were required. This allowed the formation of new salt

493   bridges and hydrogen bonds between the sugar and the α-helical structure including the residue

494   N614 (Asn615) and Gln563 which is present on an adjacent loop (Fig 11A,B). This data suggest

495   that inhibition of Aconitase activity, through siltation of Aspargine 612, is due to major distortion

496   of the active site which prevents catalysis from occurring.

497

498   Discussion

499   Despite the importance of capacitation, the molecular mechanisms underlying this process are not

500   yet fully understood. Previous studies have suggested that one facet of capacitation is a loss in Sia

501   residues, which may be modulated by one (humans) or two (mouse) neuraminidases, namely

502 neuraminidase 1 and 3 [27]. In the present study, using a LC-MS/MS-based approach, we were

503 able to investigate capacitation-related changes of N-linked glycoproteins bearing terminal Sia.

504 Surprisingly, we found very little regulation of Sia within proteins groups following *in vitro*

505 capacitation, with only 6.3% (9 of 142 peptides) demonstrating a significant change.

506 According to our data, the enzyme EL is one of the sperm proteins in which the Sia content is

507 altered during capacitation. Previous studies have shown that four (N62, N118, N375, and N473)

508 of the five potential N-glycosylation sites of human EL are occupied by glycan moieties [51, 52].

509 In the present study, the sugar moiety at the N62 glycosylation site of EL was found to contain Sia

510 in its structure. In addition, the peptide containing this glycosylation site was significantly reduced

511 after *in vitro* capacitation, despite the fact that both quantity and molecular weight of EL remained

512 unchanged. This suggests that a loss of a small glycan moiety or of a Sia residue itself occurs

513 within EL during capacitation. Notably, a sialylated N-glycan structure at the corresponding

514 glycosylation site (N64) has also been identified by our group in the EL of rat sperm [33]. In this

515 case, spermatozoa were taken from the caput, corpus and cauda regions of the epididymis.

516 Remarkably, the Sia residue within EL was only found in spermatozoa derived from the caudal

517 location. Furthermore, we have observed that the amount of EL within rat spermatozoa does not

518 change, suggesting that Sia is added to EL during epididymal transit (**data not published;** [33]).

519 Given that Sia residues are removed from the same glycosylation site during capacitation, it is

520 likely that this glycan moiety plays a specific role in regulating EL enzyme activity.

521 The glycosylation site at N62 of mouse EL is a conserved feature among animals and other

522 members of the triglyceride lipase gene family, such as lipoprotein lipase and hepatic lipase. Using

523 recombinant proteins, two separate studies have produced point mutations of the amino acids that

524 are glycosylated in EL. Interestingly, in both cases, the loss of N62 led to increased EL activity

525   [51, 52]. Due to their negative charge and hydrophilicity, Sia residues within this glycan moiety

526   could influence the structure and/or substrate specificity of EL, therefore, regulating its enzymatic

527   activity. Of note however, we observed a decrease in the PLA_1 activity of EL following reduction

528   of its sialylated glycopeptides (N62 glycosylation site) during capacitation. We can only assume

529   that, besides the loss of N62, EL is likely to be regulated in other (as yet unknown) ways in order

530   to switch off its activity.

531   In addition to EL, we found N612 sialytion of ACO2 increase following *in vitro* capacitation. This

532   enzyme catalyzes the non-redox reaction of the TCA cycle in which stereo-specific isomerization

533   of citrate to isocitrate occurs [53]. Adequate supply of ATP is essential to support capacitation-

534   associated changes such as hyperactivation [54]. In mouse, it is fairly well understood that, during

535   capacitation, there is a switch from oxidative phosphorylation over to glycolysis [5]. Thus, non-

536   capacitated sperm show high oxygen consumption, which diminishes as sperm make the switch

537   over to glycolysis during capacitation [5]. Herein, such a switch could be brought about through

538   sialylation of ACO2 particularly N612. Indeed, modelling of the enzyme suggests that the Asn

539   group sits atop of the ACO2 activity site (Fig. 11) in a highly conserved region. Analyses of

540   multiple X-ray crystal structures of Aconitate hydratase has shown that a vast array of residues

541   from all four domains of the enzyme are required to carry out catalysis [55] whether it's to bind

542   and recognize substrate or ligate the [4Fe-4S] cluster. Similarly, this complex array, dependent on

543   bound ligands, displays a number of nuanced and obvious conformational changes within its active

544   site and other domains [55]. Thus, it is apparent that in our model, inhibition likely occurs through

545   segmental conformational change of the antiparallel helical motif that N612 is a part (residues 606-

546   612 in our model; Fig. 11). As this includes active site residue Arg607, it is possible changes in

547   substrate binding may occur to prevent catalysis such as a rotameric shifts or larger domain

548   movements that may prevent substrate binding and release, a trait often linked with N-linked

549   glycosylation [56]. With the observation that both the mutation to Glutamate (Glu612) and the

550   Asn612 sialic acid (N-link) modified enzymes shuts down activity of the enzyme and the former

551   modification in our models (not depicted) suggests a new salt bridge or hydrogen bond with the

552   either the sidechain amine of Gln563 or Lys605 is likely. This further underlines the potential

553   sensitivity of ACO2 activity with respect to changes to this motif with the potential they instigate

554   larger downstream changes in other domains.

555   Inspection of Uniprot suggests that the glycosylation at N612 has never been reported in

556   any other cell type and, as such, may represent a novel mechanism, attributed just to sperm cells.

557   Unfortunately, compounds to block or inhibit sialic acid transferases are not cell permeable and,

558   for this reason, we were unable to directly ascribe the significance of a lack of ACO2 activity to

559   sperm physiology. Additionally, an indiscriminate blockage of sialyltransferases would have

560   raised doubts about what other proteins/pathways could also have been co-inhibited and this

561   obfuscated the interpretation. Our leading hypothesis is that glycolysis is required for the rapid

562   movement of the sperm flagella, in a process known as hyperactivation. The latter being essential

563   for fertilization to occur. Therefore, sperm cells being transcriptionally and translationally silent

564   cells may change ACO2 activity via sialylation of this protein, which facilitates the shuttling of its

565   metabolic process from oxidative phosphorylation over to glycolysis.

566

567   **References**

568

569

570   1.   Chang MC: **Fertilizing capacity of spermatozoa deposited into the fallopian tubes**. *Nature* 1951,
571   **168**(4277):697-698.
572   2.   Visconti PE, Bailey JL, Moore GD, Pan D, Olds-Clarke P, Kopf GS: **Capacitation of mouse**
573   **spermatozoa. I. Correlation between the capacitation state and protein tyrosine**
574   **phosphorylation**. *Development* 1995, **121**(4):1129-1137.
575   3.   Visconti PE, Moore GD, Bailey JL, Leclerc P, Connors SA, Pan D, Olds-Clarke P, Kopf GS:
576   **Capacitation of mouse spermatozoa. II. Protein tyrosine phosphorylation and capacitation are**
577   **regulated by a cAMP-dependent pathway**. *Development* 1995, **121**(4):1139-1150.
578   4.   Baker MA: **Proteomics of post-translational modifications of mammalian spermatozoa**. *Cell*
579   *and tissue research* 2016, **363**(1):279-287.
580   5.   Fraser LR, Lane M: **Capacitation-and fertilization-related alterations in mouse sperm oxygen**
581   **consumption**. *Reproduction* 1987, **81**(2):385-393.
582   6.   Miki K, Qu W, Goulding EH, Willis WD, Bunch DO, Strader LF, Perreault SD, Eddy EM, O'Brien DA:
583   **Glyceraldehyde 3-phosphate dehydrogenase-S, a sperm-specific glycolytic enzyme, is required**
584   **for sperm motility and male fertility**. *Proceedings of the National Academy of Sciences* 2004,
585   **101**(47):16501-16506.
586   7.   Baker MA: **The'omics revolution and our understanding of sperm cell biology**. *Asian journal of*
587   *andrology* 2011, **13**(1):6.
588   8.   Baker MA, Nixon B, Naumovski N, Aitken RJ: **Proteomic insights into the maturation and**
589   **capacitation of mammalian spermatozoa**. *Systems biology in reproductive medicine* 2012,
590   **58**(4):211-217.
591   9.   Ficarro S, Chertihin O, Westbrook VA, White F, Jayes F, Kalab P, Marto JA, Shabanowitz J, Herr
592   JC, Hunt DF: **Phosphoproteome analysis of capacitated human sperm evidence of tyrosine**
593   **phosphorylation of a kinase-anchoring protein 3 and valosin-containing protein/p97 during**
594   **capacitation**. *Journal of Biological Chemistry* 2003, **278**(13):11579-11589.
595   10.   Porambo JR, Salicioni AM, Visconti PE, Platt MD: **Sperm phosphoproteomics: historical**
596   **perspectives and current methodologies**. *Expert review of proteomics* 2012, **9**(5):533-548.
597   11.   Brewis IA, Gadella BM: **Sperm surface proteomics: from protein lists to biological function**.
598   *MHR: Basic science of reproductive medicine* 2009, **16**(2):68-79.
599   12.   Varki A: **Biological roles of oligosaccharides: all of the theories are correct**. *Glycobiology* 1993,
600   **3**(2):97-130.
601   13.   Lowe JB, Marth JD: **A genetic approach to mammalian glycan function**. *Annual review of*
602   *biochemistry* 2003, **72**(1):643-691.
603   14.   Fei W, Hao X: **Wheat germ agglutinin (WGA) receptors on human sperm membrane and male**
604   **infertility**. *Archives of andrology* 1990, **24**(1):97-97.
605   15.   Jiménez I, Gonzalez-Marquez H, Ortiz R, Betancourt M, Herrera J, Fierro R: **Expression of lectin**
606   **receptors on the membrane surface of sperm of fertile and subfertile boars by flow cytometry**.
607   *Archives of andrology* 2002, **48**(2):159-166.
608   16.   Steele M, Wishart G: **Demonstration that the removal of sialic acid from the surface of chicken**
609   **spermatozoa impedes their transvaginal migration**. *Theriogenology* 1996, **46**(6):1037-1044.
610   17.   Yudin AI, Generao SE, Tollner TL, Treece CA, Overstreet JW, Cherr GN: **Beta-defensin 126 on the**
611   **cell surface protects sperm from immunorecognition and binding of anti-sperm antibodies**.
612   *Biology of reproduction* 2005, **73**(6):1243-1252.
613   18.   Ma X, Pan Q, Feng Y, Choudhury BP, Ma Q, Gagneux P, Ma F: **Sialylation facilitates the**
614   **maturation of mammalian sperm and affects its survival in female uterus**. *Biology of*
615   *reproduction* 2016, **94**(6):123, 121-110.

19. Tollner TL, Yudin AI, Treece CA, Overstreet JW, Cherr GN: **Macaque sperm coating protein DEFB126 facilitates sperm penetration of cervical mucus**. *Human reproduction* 2008, **23**(11):2523-2534.

20. Focarelli R, Giuffrida A, Rosati F: **Changes in the sialylglycoconjugate distribution on the human sperm surface during in-vitro capacitation: partial purification of a 20 kDa sialylglycoprotein of capacitated spermatozoa**. *MHR: Basic science of reproductive medicine* 1995, **1**(8):369-373.

21. Mahmoud A, Parrish J: **Oviduct fluid and heparin induce similar surface changes in bovine sperm during capacitation: a flow cytometric study using lectins**. *Molecular Reproduction and Development: Incorporating Gamete Research* 1996, **43**(4):554-560.

22. Medeiros C, Parrish J: **Changes in lectin binding to bovine sperm during heparin-induced capacitation**. *Molecular Reproduction and Development: Incorporating Gamete Research* 1996, **44**(4):525-532.

23. Jiménez I, González-Márquez H, Ortiz Ro, Herrera JA, García A, Betancourt M, Fierro R: **Changes in the distribution of lectin receptors during capacitation and acrosome reaction in boar spermatozoa**. *Theriogenology* 2003, **59**(5-6):1171-1180.

24. Rosado A, Velázquez A, Lara-Ricalde R: **Cell polarography. II. Effect of neuraminidase and follicular fluid upon the surface characteristics of human spermatozoa**. *Fertility and sterility* 1973, **24**(5):349-354.

25. Iqbal N, Hunter A: **Comparison of various bovine sperm capacitation systems for their ability to alter the net negative surface charge of spermatozoa**. *Journal of dairy science* 1995, **78**(1):84-90.

26. Focarelli R, Rosati F, Terrana B: **Sialylglycoconjugates release during in vitro capacitation of human spermatozoa**. *Journal of andrology* 1990, **11**(2):97-104.

27. Ma F, Wu D, Deng L, Secrest P, Zhao J, Varki N, Lindheim S, Gagneux P: **Sialidases on mammalian sperm mediate deciduous sialylation during capacitation**. *Journal of Biological Chemistry* 2012, **287**(45):38073-38079.

28. Davis BK, Byrne R, Bedigian K: **Studies on the mechanism of capacitation: albumin-mediated changes in plasma membrane lipids during in vitro incubation of rat sperm cells**. *Proceedings of the national academy of sciences* 1980, **77**(3):1546-1550.

29. Baker MA, Krutskikh A, Curry BJ, McLaughlin EA, Aitken RJ: **Identification of cytochrome P450-reductase as the enzyme responsible for NADPH-dependent lucigenin and tetrazolium salt reduction in rat epididymal sperm preparations**. *Biology of reproduction* 2004, **71**(1):307-318.

30. Baker MA, Krutskikh A, Curry BJ, Hetherington L, Aitken RJ: **Identification of cytochrome-b5 reductase as the enzyme responsible for NADH-dependent lucigenin chemiluminescence in human spermatozoa**. *Biology of reproduction* 2005, **73**(2):334-342.

31. Daniel Jr J: **Methods in mammalian embryology**. *Methods in mammalian embryology* 1971.

32. Wessel D, Flugge UI: **A method for the quantitative recovery of protein in dilute solution in the presence of detergents and lipids**. *Anal Biochem* 1984, **138**(1):141-143.

33. Villaverde AISB, Hetherington L, Baker MA: **Quantitative glycopeptide changes in rat sperm during epididymal transit**. *Biology of reproduction* 2016, **94**(4):91, 91-13.

34. Baker MA, Naumovski N, Hetherington L, Weinberg A, Velkov T, Aitken RJ: **Head and flagella subcompartmental proteomic analysis of human spermatozoa**. *Proteomics* 2013, **13**(1):61-74.

35. Darrow AL, Olson MW, Xin H, Burke SL, Smith C, Schalk-Hihi C, Williams R, Bayoumy SS, Deckman IC, Todd MJ: **A novel fluorogenic substrate for the measurement of endothelial lipase activity**. *Journal of lipid research* 2011, **52**(2):374-382.

36. McCoy MG, Sun G-S, Marchadier D, Maugeais C, Glick JM, Rader DJ: **Characterization of the lipolytic activity of endothelial lipase**. *Journal of lipid research* 2002, **43**(6):921-929.

663 37.   Seu KJ, Cambrea LR, Everly RM, Hovis JS: **Influence of lipid chemistry on membrane fluidity: tail**
664   **and headgroup interactions**. *Biophysical journal* 2006, **91**(10):3727-3735.
665 38.   Dawaliby R, Trubbia C, Delporte C, Noyon C, Ruysschaert J-M, Van Antwerpen P, Govaerts C:
666   **Phosphatidylethanolamine is a key regulator of membrane fluidity in eukaryotic cells**. *Journal*
667   *of Biological Chemistry* 2016, **291**(7):3658-3667.
668 39.   McCallum CD, Epand RM: **Insulin receptor autophosphorylation and signaling is altered by**
669   **modulation of membrane physical properties**. *Biochemistry* 1995, **34**(6):1815-1824.
670 40.   Inoue N, Hirata K, Yamada M, Hamamori Y, Matsuda Y, Akita H, Yokoyama M:
671   **Lysophosphatidylcholine inhibits bradykinin-induced phosphoinositide hydrolysis and calcium**
672   **transients in cultured bovine aortic endothelial cells**. *Circulation research* 1992, **71**(6):1410-
673   1421.
674 41.   Lundbaek JA, Andersen OS: **Lysophospholipids modulate channel function by altering the**
675   **mechanical properties of lipid bilayers**. *The Journal of general physiology* 1994, **104**(4):645-673.
676 42.   Owens K, Kennett FF, Weglicki WB: **Effects of fatty acid intermediates on Na+-K+-ATPase**
677   **activity of cardiac sarcolemma**. *American Journal of Physiology-Heart and Circulatory Physiology*
678   1982, **242**(3):H456-H461.
679 43.   Salicioni AM, Platt MD, Wertheimer EV, Arcelay E, Allaire A, Sosnik J, Visconti PE: **Signalling**
680   **pathways involved in sperm capacitation**. *Society of Reproduction and Fertility supplement*
681   2007, **65**:245.
682 44.   Roldan E, Shi Q: **Sperm phospholipases and acrosomal exocytosis**. *Front Biosci* 2007, **12**(1):89-
683   104.
684 45.   Lloyd S, Lauble H, Prasad G, Stout C: **The mechanism of aconitase: 1.8 Å resolution crystal**
685   **structure of the S642A: citrate complex**. *Protein Science* 1999, **8**(12):2655-2662.
686 46.   Lauble H, Kennedy M, Emptage M, Beinert H, Stout C: **The reaction of fluorocitrate with**
687   **aconitase and the crystal structure of the enzyme-inhibitor complex**. *Proceedings of the*
688   *National Academy of Sciences* 1996, **93**(24):13699-13703.
689 47.   Lauble H, Kennedy MC, Beinert H, Stout CD: **Crystal structures of aconitase with trans-aconitate**
690   **and nitrocitrate bound**. *Journal of molecular biology* 1994, **237**(4):437-451.
691 48.   Robbins A, Stout C: **Structure of activated aconitase: formation of the [4Fe-4S] cluster in the**
692   **crystal**. *Proceedings of the National Academy of Sciences* 1989, **86**(10):3639-3643.
693 49.   Beinert H, Kennedy MC, Stout CD: **Aconitase as iron− sulfur protein, enzyme, and iron-**
694   **regulatory protein**. *Chemical reviews* 1996, **96**(7):2335-2374.
695 50.   Dupuy J, Volbeda A, Carpentier P, Darnault C, Moulis J-M, Fontecilla-Camps JC: **Crystal structure**
696   **of human iron regulatory protein 1 as cytosolic aconitase**. *Structure* 2006, **14**(1):129-139.
697 51.   Miller GC, Long CJ, Bojilova ED, Marchadier D, Badellino KO, Blanchard N, Fuki IV, Glick JM,
698   Rader DJ: **Role of N-linked glycosylation in the secretion and activity of endothelial lipase**.
699   *Journal of lipid research* 2004, **45**(11):2080-2087.
700 52.   Skropeta D, Settasatian C, McMahon MR, Shearston K, Caiazza D, McGrath KC, Jin W, Rader DJ,
701   Barter PJ, Rye K-A: **N-Glycosylation regulates endothelial lipase-mediated phospholipid**
702   **hydrolysis in apoE-and apoA-I-containing high density lipoproteins**. *Journal of lipid research*
703   2007, **48**(9):2047-2057.
704 53.   Beinert H, Kennedy MC: **Aconitase, a two-faced protein: enzyme and iron regulatory factor**.
705   *The FASEB journal* 1993, **7**(15):1442-1449.
706 54.   Ferramosca A, Zara V: **Bioenergetics of mammalian sperm capacitation**. *BioMed research*
707   *international* 2014, **2014**.
708 55.   Lauble H, Stout CD: **Steric and conformational features of the aconitase mechanism**. *Proteins:*
709   *Structure, Function, and Bioinformatics* 1995, **22**(1):1-11.

710   56.   Imperiali B, O'Connor SE: **Effect of N-linked glycosylation on glycopeptide and glycoprotein**
711   **structure**. *Current opinion in chemical biology* 1999, **3**(6):643-649.

712

713

714   **Figure Legends:**

715

716   **Figure 1.** Immunoblotting of mouse cauda sperm previously incubated in non-capacitating (N-

717   Cap) or capacitating media supplemented (Cap-H) or not (Cap) with the PKA inhibitor H89.

718   Protein extraction was performed in SDS-PAGE buffer and 10 μg was loaded per lane. Membranes

719   were probed with anti-Phosphotyrosine PT66 antibody and then re-probed with anti-α-tubulin. The

720   data show one replicate that has been repeated in 6 biological replicates.

721

722   **Figure 2.** Schematic representation of the strategy used to identify and quantify sialylated N-linked

723   glycopeptides extracted from mouse sperm. Deamidated asparagine residue (-D).

724

725   **Figure 3.** Immunoblot analysis of cauda spermatozoa from mouse. Sperm samples were incubated

726   in non-capacitating (N-Cap) or capacitating media supplemented (Cap-H) or not (Cap) with the

727   PKA inhibitor H89. Extraction was performed using SDS-PAGE buffer and 15 μg of protein was

728   loaded per lane. **(A)** Membranes were probed with anti-EL and then **(B)** re-probed with anti-α-

729   tubulin. **(C)** Graphic below shows relative immunoreactivity levels of both EL (left) and α-tubulin

730   (right). No statistical difference was observed among groups, which consist of five biological

731   replicates each.

732

733 **Figure 4**. Immunofluorescent localization of EL and the corresponding phase-contrast

734 micrographs of non-capacitated and capacitated mouse sperm cells. (**a-d'**) Fixed spermatozoa were

735 immobilized on pre-coated slides, permeabilized with ice cold methanol and incubated overnight

736 with anti-EL antibody. Alexa Fluor 488-conjugated secondary antibody was used for detection of

737 the primary antibody. Primary antibody was omitted in control (e and f). The scale bars represent

738 20 μm. The experiment was repeated using four biological replicates.

739

740 **Figure 5**. Assessment of acrosomal status by FITC-PNA labelling of non-capacitated (black and

741 grey bars) and capacitated (hatched and dotted bars) mouse sperm either with (grey and dotted

742 bars) or without (black and hatched bars) previous incubation with calcium ionophore A23187.

743 Sperm were counted for intact, partial or complete acrosome reaction. The data were expressed as

744 mean ± SE. Different letters represent statistical differences ($p < 0.01$) between treatments within

745 each category (intact, partial or complete acrosome reaction). The graph represents the average of

746 5 biological replicates.

747

748 **Figure 6.** Phospholipase A_1 (PLA_1) activity and the effect of the addition of A23187 and the PKA

749 inhibitor H89 on non- and capacitated mouse spermatozoa. Enzyme activity was measured using

750 the fluorescent PED-A_1 substrate. **(A)** PLA_1 activity rate, within the first 10 min, for sperm cells

751 previously incubated in non-capacitating or capacitating media with or without H89 and A23187.

752 Image represents the mean value of five biological experiments. **(B)** Example of the raw data for

753 two non-capacitated (solid line) and two capacitated (dotted line) samples.

754

755   **Figure 7.** Decrease in Aconitase activity during capacitation. Spermatozoa from mice were

756   retrieved and incubated under non- or capacitating conditions. Following protein extraction,

757   Aconitase activity was measured. To ensure equal amounts of Aconitase were present, the lysate

758   was precipitated, run into SDS page, transferred and probed using anti-Aconitase antibody. The

759   data shown is the average ($\pm$ SD) of four biological replicates. Asterisk represents statistical

760   significance ($p < 0.01$).

761

762   **Figure 8.** Following cloning and insertion of the Aconitase gene into plasmid, site directed

763   mutagenesis was used to create the N612E mutant. **(A-D)** HEK293 cells were transiently

764   transfected with GFP-tagged WT **(A,C)** or N612E mutant **(B,D).** Both anti-GFP tag fluorescent

765   **(A,B)** and phase **(C,D)** images were taken. Scale bar = 50 μM. **(E-F)** Transfected cells were run

766   through flow cytometer. Shown is the FL-1 channel vs counts of **(E)** GFP-tagged WT or **(F)** GFP-

767   tagged N612E mutant. Arrow points to the mean signal intensity for each sample. Horizontal line

768   represents the gate used for cell counting. **(G)** shows signal from non-transfected cells**.**

769

770   **Figure 9.** HEK293 cells were transfected with either $(His)_6$-tagged WT or $(His)_6$-tagged N612E

771   mutant for Aconitase. Cells were lysed and recombinant Aconitase purified on nickel beads.

772   Following elution, samples were run and probed with **(G)** anti-$(His)_6$-tagged protein or **(H)** anti-

773   Aconitase. Control samples comprise non-transfected cells.

774

775 **Figure 10.** N612E-mutant Aconitase displays no activity**.** HEK293 cells were transiently

776 transfected with (His)$_6$-tagged WT and (His)$_6$-tagged N612E mutant. Aconitase was purified over

777 nickel beads, run in SDS-PAGE and the immunoblotting performed to ensure that equal amounts

778 of protein were used. Bars demonstrate the average (n=6) activity of Aconitase with SD. Non-

779 transfected cells were used as controls.

780 **Figure 11.** (A) Ball and stick together with (B) ribbon model of aconitase. The different amino

781 acids are labelled as shown. The purple dotted line represents hydrogen bonding. Shown is sialic

782 acid docked onto aspargine 612.

783

784 **Table 1.** List of sialylated N-glycopeptides identified in non-capacitated and capacitated mouse

785 sperm and their regulation during the process of capacitation.

786

Protein ID	Peptide sequence	Mascot score	Fold change	p Value	MS/MS (suppl 1)
Angiotensin-converting enzyme	K.EADNFFTSLGLLPVPPEFW**NK.S**	42.9	ND	ND	1
	K.LITGQP**NMS**ASAMMNYFKPLTE WLVTENR.R *	40.7	ND	ND	2
	K.STEVS**NHT**LK.Y	54.0	-1.09	0.063	3
	K.TFDVSNFQ**NSS**IK.R	76.9	-1.34	0.074	4
Aconitate hydratase, mitochondrial precursor	R.GHLD**NIS**NNLLIGAINIENGK.A *	67.8	2.04	0.016	5
Acrosin precursor	R.VDLIDLDLC**NST**QWYNGR.V	128.0	-1.15	0.113	6

Protein	Peptide				#
ADAM 26A	R.KEKNECDLPEWC**NGT**SAECPGD VYK.A	80.8	-1.32	0.243	7
ADAM 24	K.LS**NCS**YEVLWAHMI**NK.S**	49.5	ND	ND	8
ADAM 2 precursor	R.AFS**NCS**MEDFSK.F	85.7	ND	ND	9
	R.**NTT**DYVGATYQGK.M	56.0	ND	ND	10
ADAM 5	K.A**NLS**VAYAQIR.D	80.8	1.09	0.314	11
ADAM 1b	K.EGDVCRPADGPCDLEEYC**NGT**S AACPSDR.K	82.6	-1.52	0.081	12
Anthrax toxin receptor-like	K.DFYQV**NIS**GHGL**NNT**SNMK.Q *	62.2	1.53	0.162	13
Beta-2-glycoprotein 1 precursor	K.DYRPSAG**NNS**LYQDTVVFK.C	59.2	1.12	0.264	14
	K.**NIS**FACNPGFFL**NGT**SSSK.C *	116.5	2.06	0.163	15
Sodium/potassium-transporting ATPase subunit beta-3	K.EE**NAT**IATYPEFGVLDLK.Y	85.2	-1.27	0.162	16
Basigin precursor	K.SQLTISNLDVNVDPGTYVC**NAT**N AQGTTR.E *	63.4	1.19	0.063	17
	K.TSDTGEEEAIT**NST**EANGK.Y	151.1	-1.35	0.090	18
Bactericidal permeability-increasing protein	K.T**NAS**LEVDAEENR.L	92.0	-1.27	0.214	19
C4b-binding protein	K.ALCQKPEVG**NGT**LSDEK.D	52.8	-1.30	0.233	20
	R.CEQEASEDLKPALTG**NK.T**	43.1	ND	ND	21
	R.LACL**NGT**VLR.G	76.8	-3.62	0.009	22
Carbonic anhydrase 4 precursor	R.Y**NGS**LTTPNCDETVIWTVYK.Q	88.6	1.71	0.088	23
Carboxypeptidase A5 precursor	K.AGFGG**NGS**NKNPCSETYR.G *	40.3	ND	ND	24
Carboxypeptidase Q	K.EVMNLLQPL**NVT**K.V	80.1	1.43	0.266	25

CD109 antigen homolog precursor	R.FLVTAPGIIRPGA**NVT**IGVDLLEN SPPQVLVK.A *	51.9	-2.03	0.084	26
CD151 antigen	K.LQQEFHCCGS**NNS**QDWQDSEWI R.S	85.7	-1.03	0.466	27
CD59B glycoprotein	K.I**NTT**CSPNLDSCLYAVAGR.Q	89.4	1.02	0.466	28
Clusterin precursor	K.AFPEVC**NET**MMALWEECKPCLK .H *	46.9	-2.55	0.164	29
	R.QEL**NDS**LQVAER.L	72.9	ND	ND	30
Choline transporter-like protein 5	R.CIPDLSAL**NGT**WTPGSR.M	84.3	1.11	0.312	31
Cation channel sperm-associated protein subunit gamma 2	K.LY**NMS**GDYGIPDLFFLDK.G	63.9	-1.30	0.163	32
	R.GVD**NST**YCDYK.L	73.8	ND	ND	33
Cation channel sperm-associated protein subunit beta	K.TPVYNPLGL**NLT**IQGSELFHFK.V *	66.5	ND	ND	34
CUB and zona pellucida-like domain-containing protein 1 precursor	K.ALVLQLSANE**NCT**WTIERPE**NR.S** *	122.2	-1.72	0.181	35
	K.GFSASYTSIYIHDV**NTT**SLSCVSD K.M	89.8	1.77	0.146	36
Dickkopf-like protein 1 precursor	K.VTD**NQT**GEVLISEK.V	79.2	1.04	0.460	37
Dipeptidase 3 precursor	R.HHFYT**NIS**GLTSFGEK.V	101.5	-1.30	0.122	38
	R.MCSAYPELELVTSADGL**NNT**QK. L	150.4	-1.08	0.434	39
Embigin precursor	K.KDDEPLETTGDF**NTT**K.M	75.9	1.42	0.338	40
	K.YII**NGS**HA**NET**R.L	68.4	ND	ND	41
Endoplasmin precursor	K.HN**NDT**QHIWESDSNEFSVIADPR. G *	93.0	-3.89	0.200	42

	R.TDDEVVQREEEAIQLDGL**NAS**QIR.E	85.2	ND	ND	43
Equatorin	K.AV**NET**AVSMDDK.D	96.8	-1.29	0.145	44
	K.DQFFQPIPASDL**NAT**NEDK.L	101.8	1.23	0.241	45
Carboxylesterase 5A	K.HDLQVVANVCDC**NVS**DSK.A	103.1	-1.43	0.323	46
Interferon-induced guanylate-binding protein 1	K.LQEQERLLKQGFQ**NES**LQLR.Q	42.0	-1.22	0.201	47
Glycerophosphodiester phosphodiesterase domain-containing protein 4	K.EVLPSAAG**NHT**SNF**NWT**FLSTLNAGK.W *	91.7	-1.02	0.469	48
Gamma-glutamyltranspeptidase 1 precursor	R.LA**NTT**MF**NNS**K.D	56.2	ND	ND	49
Gamma-glutamyltransferase 7	R.TA**NHS**APSLENSVQPGK.R	49.2	ND	ND	50
Beta-galactosidase-1-like protein	R.CGSLQGLYTTIDFGPAD**NVT**R.I *	45.6	ND	ND	51
Solute carrier family 2, facilitated glucose transporter member 3	K.DFL**NYT**LEER.L	69.6	-1.10	0.271	52
Hexokinase-1	K.SQ**NVS**MESEVYDTPENIVHGSGSQLFDHVAECLGDFMEK.R *	94.2	ND	ND	53
Hyaluronidase PH-20 precursor	K.VG**NAS**DPVPIFVYIR.L	60.6	-1.53	0.102	54
Hypoxia up-regulated protein 1	R.AEPPL**NAS**AGDQEEK.V	61.0	-4.07	0.165	55
	R.VFGSQ**NLT**TVK.L	76.2	ND	ND	56
Izumo sperm-egg fusion protein 1 precursor	R.VWE**NSS**ETLIAK.G	85.7	-1.24	0.129	57
Casein kinase I isoform gamma-2	K.NQAL**NST**NGELNTDDPTAGHSNAPIAAPAEVEVADETK.C *	92.2	-1.32	0.210	58
Laminin subunit alpha-1 precursor	K.LDELK**NLT**SQFQESVD**NIT**K.Q *	50.0	ND	ND	59

Lysosome-associated membrane glycoprotein 1 precursor	R.AF**NIS**P**NDT**SSGSCGINLVTLK.V *	61.4	-3.42	0.113	60
	R.L**NMT**LPDALVPTFSIS**NHS**LK.A *	65.8	ND	ND	61
Epididymal-specific lipocalin-8 precursor	K.AVY**NSS**GSCVTESSLGSER.D	109.7	-1.41	0.162	62
Endothelial lipase	K.DPEQEGC**NLS**LGDSK.L *	79.3	ND	ND	63
	K.IEL**NAT**NTFLVYTEEDLGDLLK.M	71.2	ND	ND	64
	K.LLENCGF**NMT**AK.T	62.7	-1.33	0.011	65
Lipid phosphate phosphohydrolase 1	K.**INCS**DGYIEDYICQGNEEK.V	120.3	1.06	0.359	66
Leucine-rich repeat-containing protein 52 precursor	K.YVFA**NTT**SLR.Y	52.5	ND	ND	67
	R.L**NIS**HNPHLLYLDK.Y	40.6	ND	ND	68
Ly6/PLAUR domain-containing protein 4 precursor	K.FQAGNL**NTT**FLIMGCAR.D	118.3	1.14	0.299	69
	R.SYLCN**NLT**NLEPFVR.L *	76.6	-1.19	0.270	70
Lysosomal alpha-mannosidase	R.DDYRPTWTL**NQT**EPVAGNYYPVNTR.I *	49.0	ND	ND	71
Epididymis-specific alpha-mannosidase precursor	K.QFF**NAS**VQFDNMDPLLDYINQR.T *	57.0	-2.59	0.155	72
	K.Y**NLT**L**NDT**SIVHPVLWLMLGPK.S	89.7	1.23	0.243	73
Membrane cofactor protein precursor	K.**NGT**HTLTDINVFK.Y	54.3	1.05	0.384	74
Mitochondria-eating protein	R.DNSPDQDQHQSD**NES**FSETQPTQVQDDLAESGK.S *	61.5	-1.69	0.127	75
Membrane metallo-endopeptidase-like 1	K.NGNMLDWWS**NFS**AR.H	63.0	-1.91	0.118	76
	R.EEMAEVLELETHLA**NAT**VPQEK.R	56.9	-1.24	0.362	77

	R.VLIDLFIWNDDQ**NSS**R.H	58.9	ND	ND	78
Ecto-ADP-ribosyltransferase 3	R.KGTSNDLVLQSI**NST**CSYYECAFL GGLK.T *	86.0	-1.18	0.320	79
	R.LG**NFT**LAYSAKPETADNQR.V *	112.9	1.19	0.079	80
Nicastrin	K.DLYEYSWVQGPWNS**NR.T** *	45.9	ND	ND	81
L-amino-acid oxidase precursor	K.VVTLGL**NR.T**	55.6	-1.34	0.138	82
	R.TLGL**NLT**QFTQYDENTWTEVHN VK.L	97.3	-1.10	0.418	83
Nuclear pore membrane glycoprotein 210-like precursor	K.CFP**NSS**VIEEDGGGLLR.S	99.7	-1.16	0.352	84
	K.EYFEEQLSTS**NGS**YHVVK.A	44.4	-1.90	0.069	85
	K.SS**NET**LAHFEDSK.S	83.2	-1.38	0.051	86
	R.EVVV**NAS**SR.L	58.7	1.01	0.470	87
	R.G**NST**ILAR.D	68.4	-1.78	0.179	88
	R.ILIPFIPGFYM**NQS**EFVLGHK.D	45.3	-1.05	0.467	89
	R.KFD**NFS**SLMLEWK.S	66.6	-1.10	0.315	90
Lysosomal Pro-X carboxypeptidase precursor	K.**NIS**SHSNIIFSNGELDPWSGGGVT R.D *	91.7	ND	ND	91
Protein disulfide-isomerase-like protein of the testis	K.ALLF**NNS**DEVADFVK.S	82.0	-2.69	0.235	92
Phospholipase B1, membrane-associated	K.AE**NLT**SQVR.T	73.6	1.11	0.268	93
	K.NSNLG**NGT**WMVCEER.A	89.7	-1.67	0.053	94
	K.TLE**NVT**TLPNILR.K	42.1	1.00	0.499	95
	R.D**NFT**VVVQPLFE**NVS**MPR.T *	58.5	ND	ND	96
	R.HSQ**NLT**AMQELK.K	78.2	-1.38	0.153	97
	R.DQG**NVT**DMASMK.Y	89.4	-1.10	0.326	98

Putative phospholipase B-like 1	R.F**NET**LHR.G	49.8	-1.23	0.200	99
Prominin-1 precursor	K.DALQ**NMS**SSLK.S	50.1	ND	ND	100
	K.SLQDAATQLNT**NLS**SVR.N	121.1	-1.46	0.244	101
Inactive serine protease 39	R.ILLGYNQLSNPS**NYS**R.Q	104.5	-2.00	0.001	102
Serine protease 42	K.LQHPV**NFT**TNIYPVCIPSESFPVK. A *	84.1	1.22	0.217	103
Serine protease 44	K.GGDACQGDSGGPLVCEF**NK.T**	97.1	-1.61	0.067	104
Serine protease 46	K.VGVQTLPD**NST**SELLVTR.I	100.3	1.15	0.349	105
Serine protease 52	R.NCWVTGWGIT**NTS**EK.G	101.7	-3.09	0.003	106
Prostaglandin-H2 D-isomerase precursor	K.TVVAPSTEGGL**NLT**STFLR.K	141.6	-1.42	0.279	107
Patched domain-containing protein 3	K.VVQE**NGT**QILYQEVCAK.Y	94.7	1.14	0.192	108
	R.FVQGHFST**NDT**YR.F	60.9	-1.17	0.324	109
Pituitary tumor-transforming gene 1 protein-interacting protein precursor	R.VGCSEYT**NR.S**	59.5	-1.02	0.432	110
RING finger protein 126	R.NTE**NGS**APSTAPTDQNR.Q	75.4	ND	ND	111
Solute carrier family 13 member 5	R.AMFNLDNFPDWA**NST**SVNT.-	100.3	1.03	0.472	112
Solute carrier family 22 member 21	R.IPDTV**NLS**SAWR.N	91.2	-1.09	0.201	113
	R.LATIA**NFS**ELGLEPGR.D	96.2	-1.11	0.282	114
Sperm acrosome membrane-associated protein 1 precursor	K.LLKPDQQPVILT**NDS**AVLEITR.E	138.6	1.38	0.258	115
Saccharopine dehydrogenase-like oxidoreductase	K.ACIE**NGT**SCIDICGEPQFLELMHA K.Y	81.0	ND	ND	116
	R.NQM**NGT**LTAVESFLTINTGPEGL CIHDGTWK.S *	91.5	ND	ND	117

Sortilin precursor	R.HLYTTTGGETDFT**NVT**SLR.G	62.3	-2.18	0.053	118
Kunitz-type protease inhibitor 4	R.FFY**NQT**AK.Q	42.0	-1.09	0.317	119
Signal peptide peptidase-like 2B	K.SGNSIMVEVATGPS**NSS**THEK.L	87.6	1.18	0.290	120
Suppressor of G2 allele of SKP1 homolog	R.CQEIQ**NGS**ESEVSASQR.T	84.2	ND	ND	121
Synaptophysin-like protein 1	K.**NQT**VTATFGYPFR.L	89.3	-1.29	0.154	122
Testisin precursor	K.LSSPVTYNNFIQPICLL**NST**YK.F	94.7	-1.35	0.194	123
Testis-expressed sequence 29 protein	K.FAVCDIPLYDICDY**NVT**R.E	101.0	1.02	0.448	124
Transmembrane protease serine 12	R.EEG**NGT**TILQEAK.V	43.0	ND	ND	125
Testis-expressed protein 101 precursor	R.HCPTCVALGSCSSAPSMPCA**NGT**TQCYQGR.L	75.2	-1.99	0.004	126
	R.TF**NWT**SK.A	48.7	-1.91	0.001	127
	R.VPETTATS**NMS**GTR.H	93.3	-2.01	0.001	128
Ubiquitin carboxyl-terminal hydrolase 7	R.ITQNPVING**NVT**LSDGHSNAEEDMEDDTSWR.S *	109.5	ND	ND	129
Zonadhesin precursor	K.CPLGTECKDSVDGGS**NCT**K.I	51.9	ND	ND	130
	K.DAQGDLIPA**NK.T**	74.4	-1.24	0.189	131
	K.DGSS**NCT**NIPLQCPAHSR.Y	93.0	-1.14	0.183	132
	K.FQCPSETYCKDIEDGNS**NCT**R.I	43.0	ND	ND	133
	K.TCTTLCTCSAHS**NIT**CSPTACK.A	52.2	-1.04	0.236	134
	R.VGSQSSGWM**NSS**VTIPK.G	52.6	-2.06	0.009	135
Zona pellucida sperm-binding protein 3 receptor precursor	K.GVCLKPMVING**NLS**VER.V	63.8	1.58	0.191	136
	K.TYLFGHEE**NST**EHAMK.G	63.8	-1.64	0.137	137

	R.ASLNDPQTVTCQE**NLT**WSSTNGCER.I	137.3	-1.03	0.357	138
	R.LALFTFP**NIS**ET**NVT**NK.T *	95.9	1.27	0.191	139
	R.V**NSS**HLSCDE**NGS**WVYSTFCAR.K *	75.1	1.08	0.281	140
Zona pellucida-binding protein 1 precursor	R.DGTHCLQC**NNS**LVYGAK.T *	104.7	1.02	0.435	141
Zona pellucida-binding protein 2	K.GNSQI**NIT**NTGELVLK.D *	76.5	1.70	0.145	142

787

788 * ambiguous localization of deamidated residue.

789 Consensus sequence for N-glycosylation is shown underlined and in boldface.

790 Numbers in MS/MS column correspond to page in supplementary I which contains MS/MS
791 spectrum of the glycopeptides.

792 ND (not determined) is used when the area under the curve could not be measured in all samples.

Fig. 1

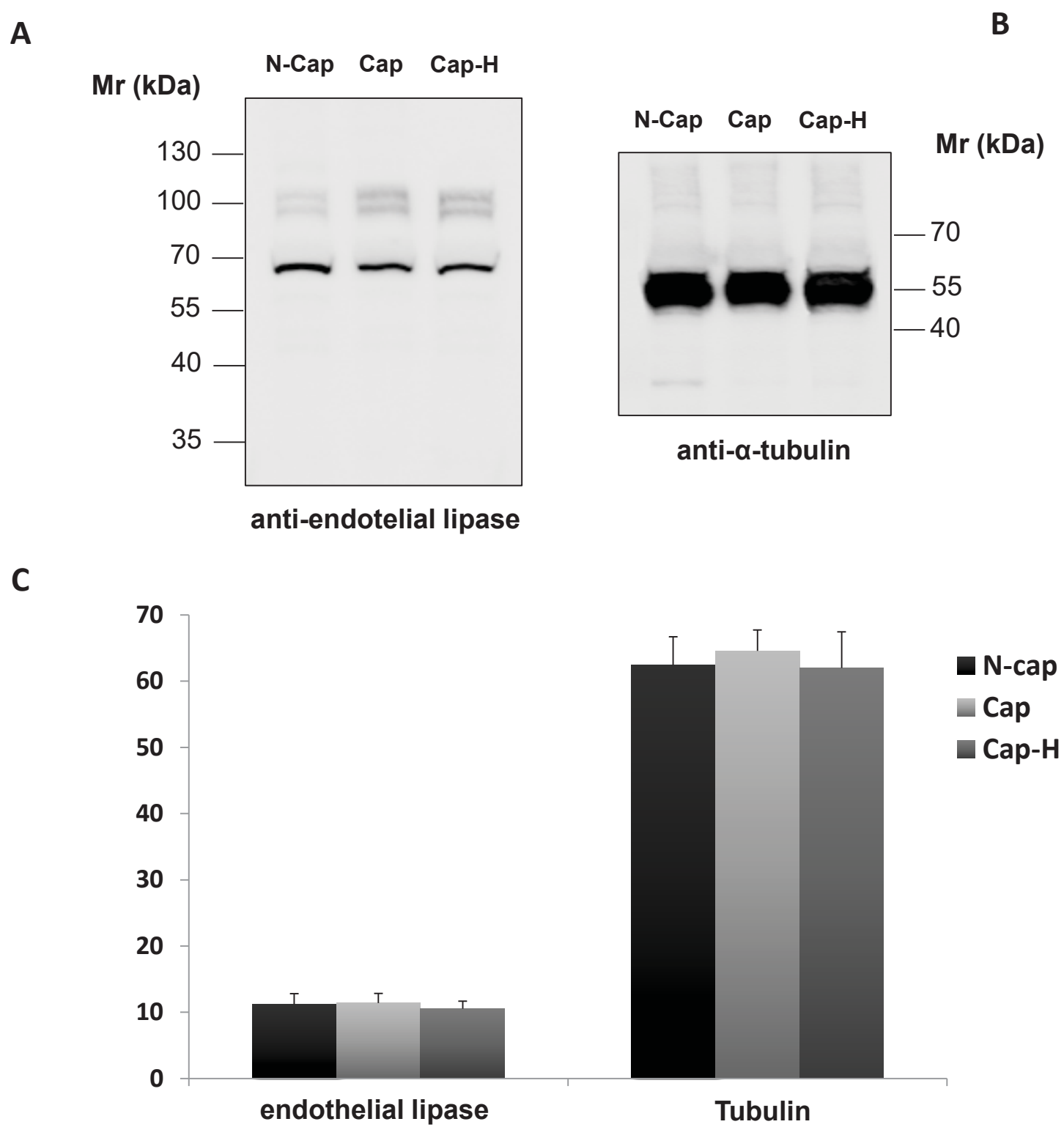| N-Cap	Cap	Cap-H

Mr (kDa)

130—

100—

70—

55—

40—

anti-Phosphotyrosine - PT66

55—

anti-α-Tubulin

Fig. 2

Non-capacitated sperm

Capacitated sperm

Sperm protein extraction and trypsinization

Sialoglycopeptides selection with titanium dioxide beads

Release of N-linked peptides by deglycosylation with PNGase F

D

D

Identification of formely N-linked sialoglycoproteins by LC-MS/MS

MS/MS spectrum

MS/MS spectrum

MS-based label-free quantification of peptides formerly bearing sialylated N-glycans

Extracted ion chromatogram

Extracted ion chromatogram

Fig. 3

A

B

Mr (kDa)

N-Cap Cap Cap-H

130 —

100 —

70 —

55 —

40 —

35 —

anti-endotelial lipase

N-Cap Cap Cap-H

Mr (kDa)

70 —

55 —

40 —

anti-α-tubulin

C

endothelial lipase   Tubulin

■ N-cap
■ Cap
■ Cap-H

Noncapacitated

Capacitated

Fig. 4

Fig. 5

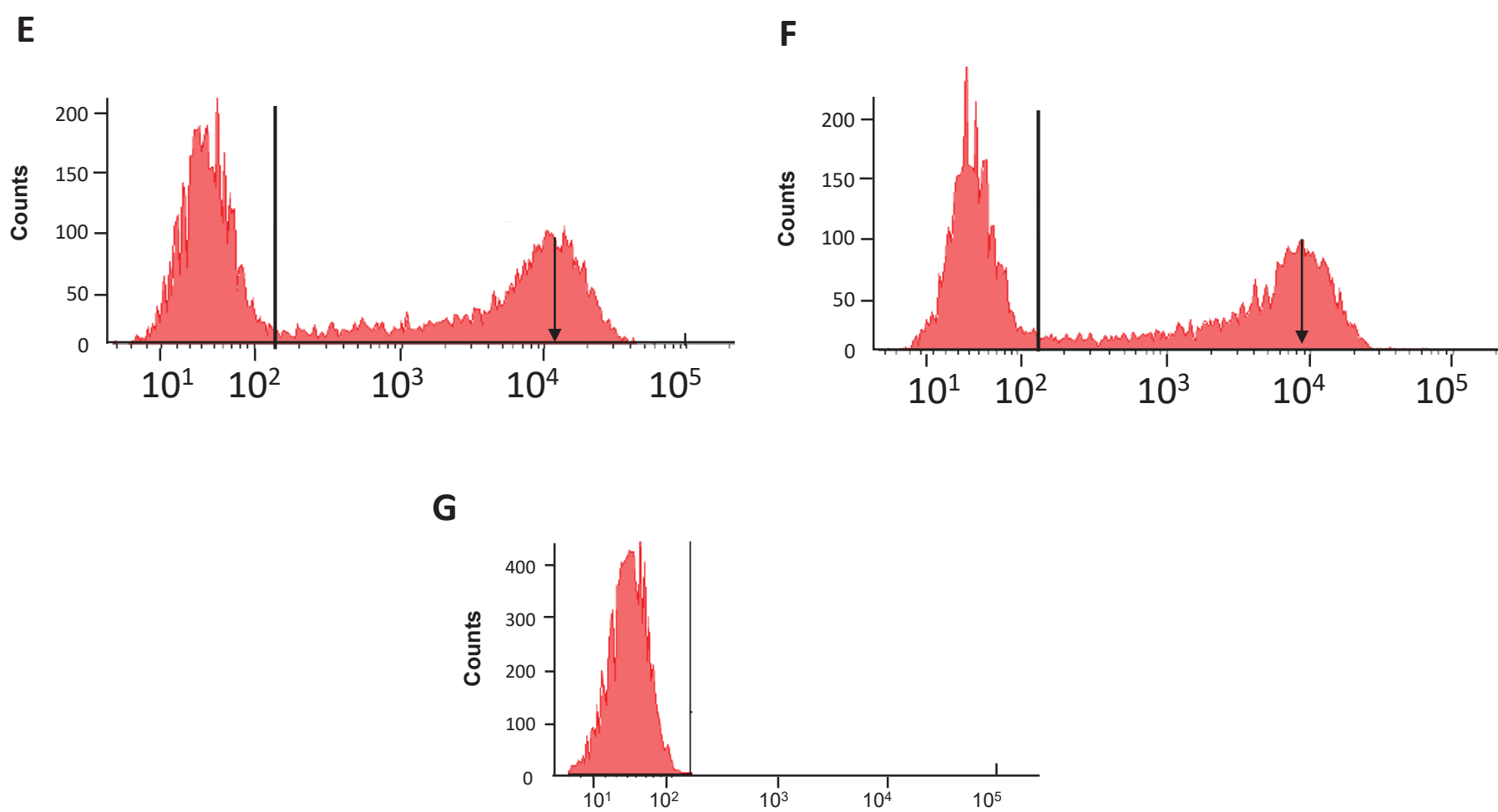Fig. 6
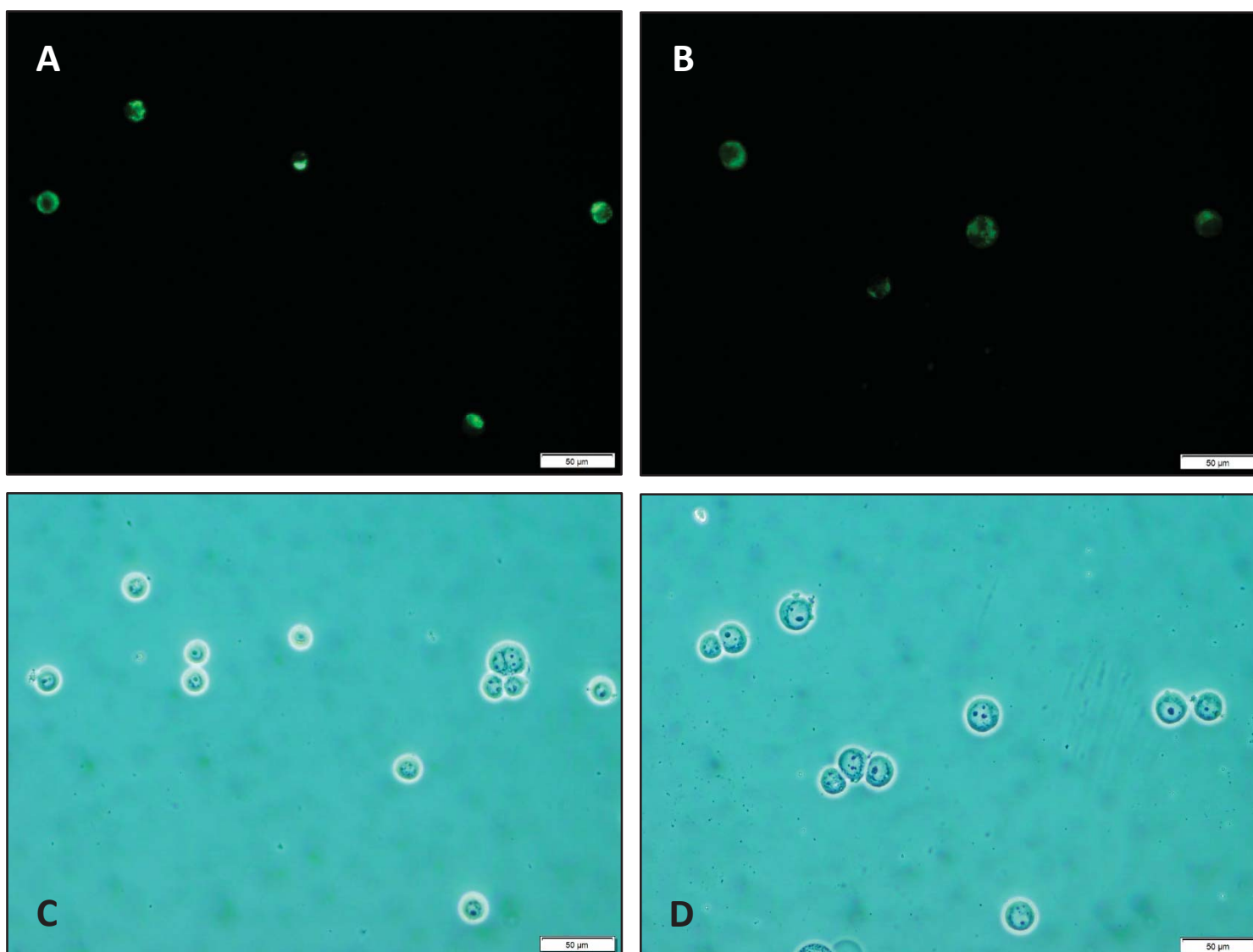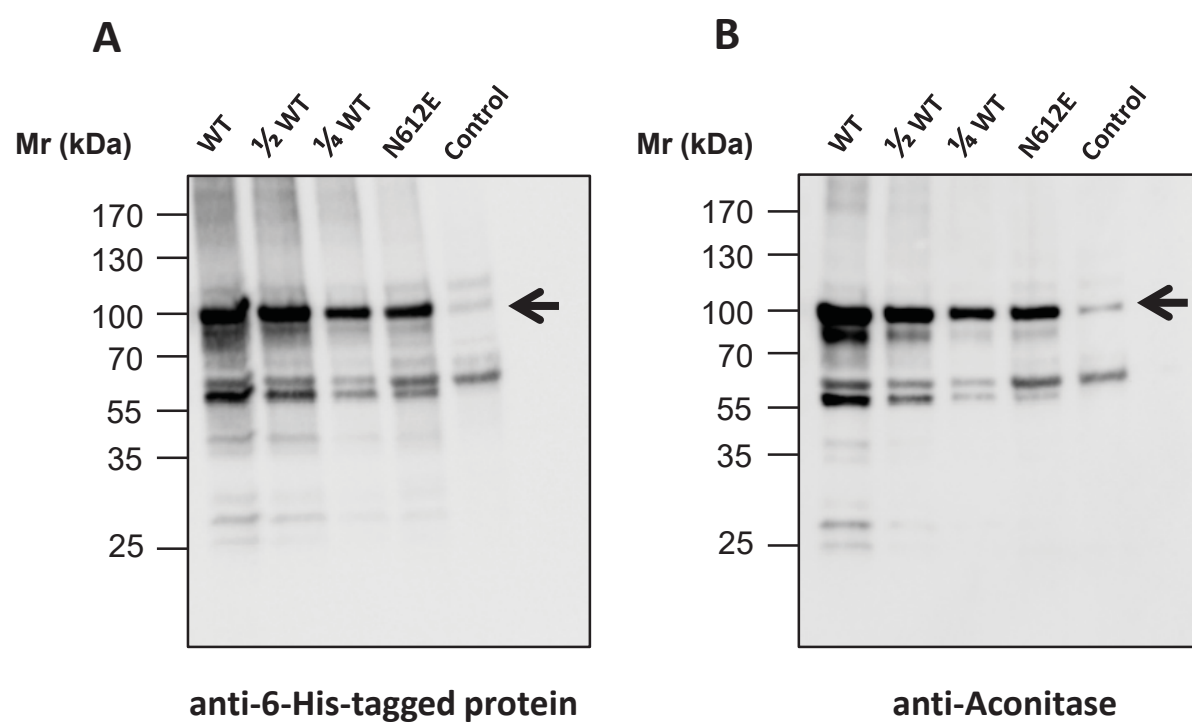
Fig. 7

Fig. 8

Wild-type Aconitase **N612E Aconitase**

Fig. 9

A

Mr (kDa)

anti-6-His-tagged protein

B

Mr (kDa)

anti-Aconitase

Fig. 10

Fig. 11

A)

B)